

Unidirectional weak visibility in band gap of 1D \mathcal{PT} -symmetric photonic crystal

Tiecheng Wang*

College of Physics and Electronic Engineering, Shanxi University, 030006, Taiyuan, China

(Dated: May 18, 2022)

We explore the scattering and absorption properties of a one-dimensional (1D) parity-time (\mathcal{PT})-symmetric photonic crystal. In addition to transmittance and reflectance, we provide a definition of the generalized absorptance to include the amplification effect of dielectrics with negative imaginary permittivity parts. Moreover, we derive the mathematical expressions of the transmittance, reflectances and absorptances from both sides of a photonic crystal with N periods. The complex band structure of this photonic crystal is studied and the corresponding evolutions of the exceptional points, \mathcal{PT} -exact phase and \mathcal{PT} -broken phase are discussed. Near the exceptional points, we find some singular behaviors, where the transmittance and reflectances from both sides are all greater than one and even reach large values simultaneously, in which case the corresponding absorptances from both sides become negative. In the band gap, a phenomenon we call unidirectional weak visibility can appear, where transmittance is zero, the reflectance from one side is very large, while the reflectance from the other side is very small. We believe that these phenomena are very beneficial for the design of optical devices.

I. INTRODUCTION

In recent years, parity-time- (\mathcal{PT})-symmetric photonic systems have attracted much interest [1, 2]. This is motivated by the study of non-Hermitian quantum mechanics [3–6], which is applied in various areas [7–9]. The non-Hermitian Hamiltonian is \mathcal{PT} -symmetric when the complex potential satisfies $V^*(-x) = V(x)$. If the eigenstate is also \mathcal{PT} -symmetric, the eigenvalue is real and the system is in a \mathcal{PT} -exact phase. Otherwise, the eigenstate is not \mathcal{PT} -symmetric, two conjugate complex eigenvalues arise and the system is in a \mathcal{PT} -broken phase. Similar characteristics to those of non-Hermitian quantum mechanics are found in optics. \mathcal{PT} -symmetric photonic systems are characterized by a complex index of refraction with a balanced gain and loss $n^*(-x) = n(x)$, have different phases and go through a phase transition from a \mathcal{PT} -exact phase to a \mathcal{PT} -broken phase at an exceptional point [10–14]. At this point, the eigenvalues coalesce and their eigenvectors become parallel.

\mathcal{PT} -symmetric photonic systems also exhibit other various intriguing regularities and phenomena. Unidirectional invisibility is a typical optical effect. It has been found that the interplay of Bragg scattering and \mathcal{PT} -symmetry allows for unidirectional invisibility in a wide range of frequencies around the Bragg point [15–19], while nonlinear optical structures also support unidirectional invisibility [20]. A \mathcal{PT} -symmetric optical medium can act simultaneously as a laser oscillator and as a coherent perfect absorber [21–25]. Through the scattering matrix formalism, the existence of a transition between \mathcal{PT} -exact scattering eigenstates and the \mathcal{PT} -broken scattering eigenstate has been reported [26]. Due to the optical reciprocity, the product of the two eigenvalues of the scattering matrix is one. In a \mathcal{PT} -exact phase,

both eigenvalues are unimodular, so the corresponding eigenstates exhibits no net amplification nor dissipation; while in a \mathcal{PT} -broken phase the unimodularity condition cannot be satisfied [27], in which case one eigenstate corresponds to amplification, and the other to dissipation. \mathcal{PT} -symmetric photonic systems violate the normal photon flux conservation but obey the generalized unitarity relations; these relations illustrate the existence of anisotropic transmission resonances [28]. Direction-dependent \mathcal{PT} -phase transition has been observed in a dielectric waveguide structure. In the forward direction, this transition is thresholdless, whereas in the backward direction it has a nonzero threshold [29–32].

We focus on \mathcal{PT} -symmetric photonic crystals. The complex band structure of one dimensional \mathcal{PT} -symmetric photonic crystals (1DPTSPC) has been calculated and analyzed, and it has been found that as the non-Hermiticity increases, two types of \mathcal{PT} -phase diagrams occur [33, 34]. The exceptional contours and band structure in the two dimensional \mathcal{PT} -symmetric photonic crystal have also been studied, whose non-Hermitian primitive cell is an integer multiple of the primitive cell of the underlying Hermitian system [35]. In previous studies, two criteria have been commonly used for differentiating the \mathcal{PT} -exact phase and \mathcal{PT} -broken phase. One is through the eigenvalues of the scattering matrix, while the other is through the eigenvalues of the effective Hamiltonian, which are revealed through the complex band structure. Actually, the first criterion differentiates further the \mathcal{PT} -exact phase for the second criterion.

Based on the previous investigations, in this paper, we study the transmission, reflection, absorption and emission properties of 1DPTSPCs. According to Bloch's theorem, these optical properties are closely related to the band structure, so we choose the second criterion to define the different phases. We provide a systematic study on the scattering and absorption properties as the non-Hermiticity increases. The rest of this paper is organized as follows, in Section II, we present our theoretical model,

* Corresponding author: tcwang@sxu.edu.cn

define the general absorptance and derive the mathematical expressions of the optical properties of 1DPTSPCs. In Section III, we analyze these optical properties for complex and real band structures. We conclude with a summary in Section IV.

II. MODEL FORMULATION

Before we study the transmittance, reflectance and absorptance of 1DPTSPCs, it is worth reviewing the properties of the generic \mathcal{PT} -symmetric photonic structure to introduce our discussion. Its transfer matrix $M(\omega)$, which relates the waves at the two sides of the structure (see the top panel in Fig. 1) has been used by many researchers [36, 37]:

$$\begin{pmatrix} C \\ D \end{pmatrix} = \begin{pmatrix} M_{11}(\omega) & M_{12}(\omega) \\ M_{21}(\omega) & M_{22}(\omega) \end{pmatrix} \begin{pmatrix} A \\ B \end{pmatrix}, \quad (1)$$

where A and D (B and C) stand for the amplitudes of the input (output) electromagnetic field from the left and right sides of the generic \mathcal{PT} -symmetric photonic structure, respectively. Following the theoretical analysis of [21], the components of the transfer matrix $M(\omega)$ satisfy $M_{22}(\omega) = M_{11}^*(\omega^*)$, $M_{12}(\omega) = -M_{12}^*(\omega^*)$ and $M_{21}(\omega) = -M_{21}^*(\omega^*)$. If the angular frequency ω is real, the transfer matrix can be parametrized as

$$M(\omega) = \begin{pmatrix} a^* & ic \\ -ib & a \end{pmatrix}, \quad (2)$$

where a is complex while b and c are real and related to each other by the condition $|a|^2 - bc = 1$. The scattering matrix $S(\omega)$ [27, 28] can be obtained by transforming the transfer matrix $M(\omega)$ into the form

$$\begin{pmatrix} B \\ C \end{pmatrix} = S(\omega) \begin{pmatrix} A \\ D \end{pmatrix} \equiv \begin{pmatrix} r_L & t \\ t & r_R \end{pmatrix} \begin{pmatrix} A \\ D \end{pmatrix}, \quad (3)$$

where $t \equiv t_L = t_R = 1/a$ are the transmission coefficients and $r_L = ib/a$ and $r_R = ic/a$ are the reflection coefficients for the left and right sides, respectively. Based on the relation between those parameters, the generalized conservation law $|T - 1| = \sqrt{R_L R_R}$ can be derived for the transmittance $T = |t|^2$ and reflectances $R_L = |r_L|^2$, $R_R = |r_R|^2$ for the left and right sides.

If the photonic structure satisfies only parity symmetry (\mathcal{P} -symmetry), then $M_{21}(\omega) = -M_{12}(\omega)$; if it possesses only time-reversal symmetry (\mathcal{T} -symmetry), $M_{22}(\omega) = M_{11}^*(\omega^*)$ and $M_{21}(\omega) = M_{12}^*(\omega^*)$ hold. Consequently, for real angular frequencies, in these two cases the reflectances from the left and right sides are equal, i.e. $R_L = R_R$. This is in contrast to \mathcal{PT} -symmetric photonic structures where for real angular frequencies in general $R_L \neq R_R$.

In order to study the optical properties of 1DPTSPCs as comprehensively as possible, we also consider the absorption or emission of the \mathcal{PT} -symmetric structure. To

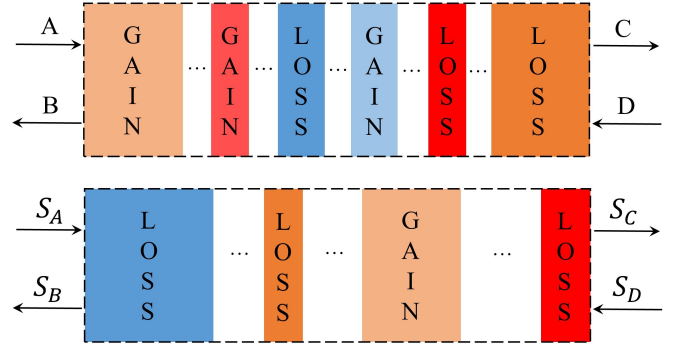


Figure 1. (Color online) Schematic pictures of a generic \mathcal{PT} photonic structure (top panel) and a generic optical structure (bottom panel). The \mathcal{PT} -symmetric photonic structure is characterized by a complex index of refraction with a balanced gain and loss, while the generic optical structure is made up of absorbing, active or both types of materials.

start with, their definitions are as follows. Consider a general optical system, as shown in the bottom panel of Fig. 1, where the energy flow densities of the light incident from its left and right sides are denoted by S_A and S_D , respectively, and those of the light emitted into the left and right sides are marked by S_B and S_C . If this system is made up of absorbing materials with positive imaginary permittivities, the energy flow density which is absorbed is $S_A + S_D - S_B - S_C$. On the other hand, if the imaginary permittivities are negative, the intensity of the light can be amplified, and the increased intensity flow is given by $S_B + S_C - S_A - S_D$. Combining these two cases, if the system is composed of absorbing, active or both types of materials, the generalized absorptance can be defined as

$$W = \frac{S_A + S_D - S_B - S_C}{S_A + S_D}. \quad (4)$$

If $W > 0$, the optical effect is absorptive; if $W < 0$, it is amplifying. When $W = 0$, the total energy flow density of the outgoing light is equal to that of the incoming light.

When the incoming light is only incident from the left or the right side, the absorptances for these two cases can be respectively expressed as

$$W_L = 1 - T - R_L, W_R = 1 - T - R_R. \quad (5)$$

Using the generalized conservation law, these absorptances can be expressed through the other reflectances as

$$W_L = 1 - T - \frac{(1 - T)^2}{R_R}, W_R = 1 - T - \frac{(1 - T)^2}{R_L}. \quad (6)$$

They hold except when $R_R = 0$ and $R_L = 0$, respectively, in which cases $T = 1$ so $W_L = -R_L$ or $W_R = -R_R$. We can also obtain the relation between W_L and W_R using the generalized conservation law, as follows:

$$W_L W_R + (T - 1)(W_L + W_R) = 0. \quad (7)$$

At the transmission resonances where $T = 1$, the incoming lights are unidirectionally reflected. This means the reflectance from one side is zero, which can be derived from the generalized conservation law. Hence, based on the definitions of W_L and W_R in Eq. (5), the absorption from this side is zero. This phenomenon can be also explained using Eq. (7), from which we can derive that the absorptances satisfy $W_L W_R = 0$ at the transmission resonances. This also means that the absorptance from one side is zero.

In our work, through the investigation of the \mathcal{PT} -symmetric photonic crystal, we offer a different view from the abovementioned works, namely that the eigenvalues of the transfer matrix $M(\omega)$ are more physically meaningful. This eigenvalue spectrum is closely related to the band structure. The complex band structure has already been explored in depth [33]. We will expound why the spontaneous symmetric breaking presented by the eigenvalue of the transfer matrix $M(\omega)$ is physically meaningful by exploring the optical scattering and absorption properties of 1DPTSPCs.

We now turn to the study on the 1DPTSPC as shown in Fig. 2(b). In our work its primitive cell (see Fig 2(a)) is composed of four layers. Their relative permittivities, which describe the balanced gain and loss, are denoted by $\varepsilon'_\alpha - i\varepsilon''_\alpha$, $\varepsilon'_\beta + i\varepsilon''_\beta$, $\varepsilon'_\beta - i\varepsilon''_\beta$ and $\varepsilon'_\alpha + i\varepsilon''_\alpha$, while their relative permeabilities are equal to one, i.e. $\mu_\alpha = \mu_\beta = 1$. The parameters $\varepsilon'_{\alpha(\beta)}$ and $\varepsilon''_{\alpha(\beta)}$ are positive real. In the remainder of this work, we use $\varepsilon''_\alpha = \varepsilon''_\beta = \varepsilon''$ for simplicity, the real parts of the relative permittivities are fixed at $\varepsilon'_\alpha = 1.1$ and $\varepsilon'_\beta = 4.0$, and the thicknesses are set to $d_\alpha = 0.35\Lambda$ and $d_\beta = 0.15\Lambda$, where Λ is the thickness of a primitive cell. Bloch's theorem essentially states the physical meaning of the eigenvalue and eigenfunction of the transfer matrix of a primitive cell

$$\begin{pmatrix} M_{11}(\omega) & M_{12}(\omega) \\ M_{21}(\omega) & M_{22}(\omega) \end{pmatrix} \begin{pmatrix} A \\ B \end{pmatrix} = e^{iK\Lambda} \begin{pmatrix} A \\ B \end{pmatrix}, \quad (8)$$

where K is the Bloch wave vector. Here and in the following, $M(\omega)$ is the transfer matrix of a generic \mathcal{PT} -symmetric primitive cell. Based on Bloch's theorem, the real [38, 39] and complex [33] band structures can be obtained. In the traditional method, the real band structure can be derived from $\cos(K\Lambda) = (M_{11}(\omega) + M_{22}(\omega))/2$. For every real frequency $\omega = \omega_a$ we can obtain the corresponding complex wave vector $K = K_a = K_{ar} + iK_{ai}$. If $K_{ai} = 0$, the eigenstate is in a conduction band, otherwise it is in a forbidden band. We call this a real band structure because the frequency here is real. The complex band structure can be obtained by expressing a Bloch state of the \mathcal{PT} -symmetric system as a linear superposition of the Bloch states of the corresponding optical system in the absence of loss and gain. Then, substituting the corresponding expression into the Helmholtz equation, for every real wave vector $K = K_c$ we obtain the corresponding complex eigenfrequency $\omega = \omega_c = \omega_{cr} + i\omega_{ci}$. If $\omega_{ci} = 0$, the system is in a \mathcal{PT} -exact phase, otherwise it is in a \mathcal{PT} -broken

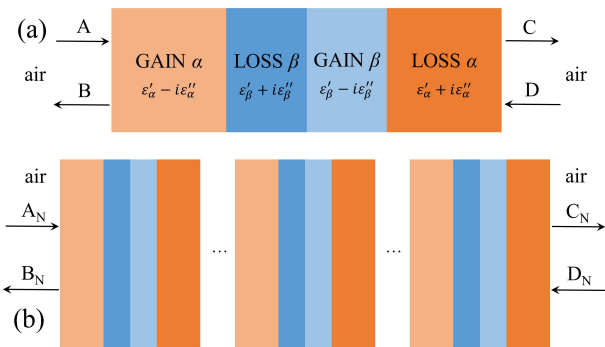


Figure 2. (Color online) Schematic picture of the 1DPTSPC, (a) shows the primitive cell made up of four layers with the relative permittivities $\varepsilon'_\alpha - i\varepsilon''_\alpha$, $\varepsilon'_\beta + i\varepsilon''_\beta$, $\varepsilon'_\beta - i\varepsilon''_\beta$ and $\varepsilon'_\alpha + i\varepsilon''_\alpha$. (b) is a depiction of a 1DPTSPC with N primitive cells, where A_N and D_N (B_N and C_N) are the amplitudes of the input (output) electromagnetic field from the left and right sides of the 1DPTSPC.

phase, in which case the transition boundary corresponds to the exceptional points. We call this a complex band structure because the frequency here is complex.

With regard to transmittance and the reflectances from both air sides of the 1DPTSPC with N primitive cells, the total transfer matrix for the model shown in Fig. 2(b) is given by

$$\begin{pmatrix} C_N \\ D_N \end{pmatrix} = \begin{pmatrix} M_{11}(\omega) & M_{12}(\omega) \\ M_{21}(\omega) & M_{22}(\omega) \end{pmatrix}^N \begin{pmatrix} A_N \\ B_N \end{pmatrix}. \quad (9)$$

Here we assume that each primitive cell is surrounded by two infinitely thin films of air on both sides. The frequency of the light is taken to be real because in this case the scattering and absorption properties have physical meanings. The N th power of a unimodular matrix $M(\omega)$ can be simplified using the following matrix identity [36]:

$$\begin{pmatrix} M_{11} & M_{12} \\ M_{21} & M_{22} \end{pmatrix}^N = \begin{pmatrix} M_{11}U_N - U_{N-1} & M_{12}U_N \\ M_{21}U_N & M_{22}U_N - U_{N-1} \end{pmatrix}, \quad (10)$$

where $U_N = \sin[(N+1)K_a\Lambda]/\sin(K_a\Lambda)$. Substituting Eq. (10) into Eq. (9) and using the parametrized form of Eq. (2) for the four-layer primitive cell, we obtain the transmission and reflection coefficients:

$$t_N = \frac{1}{aU_{N-1} - U_{N-2}}, \quad (11a)$$

$$r_{NL} = \frac{ibU_{N-1}}{aU_{N-1} - U_{N-2}}, \quad r_{NR} = \frac{icU_{N-1}}{aU_{N-1} - U_{N-2}}. \quad (11b)$$

Furthermore, using the dispersion relation, we obtain the corresponding transmittance T_N , reflectances R_{NL} and R_{NR} , and the absorptances W_{NL} and W_{NR} :

$$T_N \equiv |t_N|^2 = \frac{1}{bc \sin^2 NK_a \Lambda / \sin^2 K_a \Lambda + 1}, \quad (12a)$$

$$R_{NL} \equiv |r_{NL}|^2 = \frac{b^2}{bc + \sin^2 K_a \Lambda / \sin^2 NK_a \Lambda}, \quad (12b)$$

$$R_{NR} \equiv |r_{NR}|^2 = \frac{c^2}{bc + \sin^2 K_a \Lambda / \sin^2 NK_a \Lambda}, \quad (12c)$$

$$W_{NL} \equiv 1 - T - R_{NL} = \frac{bc - b^2}{bc + \sin^2 K_a \Lambda / \sin^2 NK_a \Lambda}, \quad (12d)$$

$$W_{NR} \equiv 1 - T - R_{NR} = \frac{bc - c^2}{bc + \sin^2 K_a \Lambda / \sin^2 NK_a \Lambda}. \quad (12e)$$

Because this photonic crystal is composed of N \mathcal{PT} -symmetric unit cells, the generalized conservation law also holds for T_N , R_{NL} and R_{NR} , while the phase relationships between transmission and reflection also hold for t_N , r_{NL} and r_{NR} . Put another way, the basic generalized unitarity relation $r_{NL}r_{NR}=t_N^2\left(1-\frac{1}{T_N}\right)$, which leads to the generalized conservation law, can be proved using the specific expressions of Eq. (11). At the frequency where $\sin(NK_a\Lambda) = 0$ and $\sin(K_a\Lambda) \neq 0$ are satisfied, from Eq. (12) we obtain

$$T_N = 1, R_{NL} = 0, R_{NR} = 0, W_{NL} = 0, W_{NR} = 0. \quad (13)$$

This case corresponds to transmission resonances which are not anisotropic.

In the abovementioned optical properties, if the frequency lies in a conduction band, then, K_a in Eqs. (10)-(12) is a real number, with $K_{ai} = 0$. On the other hand, if the frequency lies in a band gap, $K_a\Lambda = m\pi + iK_{ai}\Lambda$ (m is an integer), and the optical properties in the band gap can be derived in a similar manner:

$$T_N = \frac{1}{bc \sinh^2 NK_{ai}\Lambda / \sinh^2 K_{ai}\Lambda + 1}, \quad (14a)$$

$$R_{NL} = \frac{b^2}{bc + \sinh^2 K_{ai}\Lambda / \sinh^2 NK_{ai}\Lambda}, \quad (14b)$$

$$R_{NR} = \frac{c^2}{bc + \sinh^2 K_{ai}\Lambda / \sinh^2 NK_{ai}\Lambda}, \quad (14c)$$

$$W_{NL} = \frac{bc - b^2}{bc + \sinh^2 K_{ai}\Lambda / \sinh^2 NK_{ai}\Lambda}, \quad (14d)$$

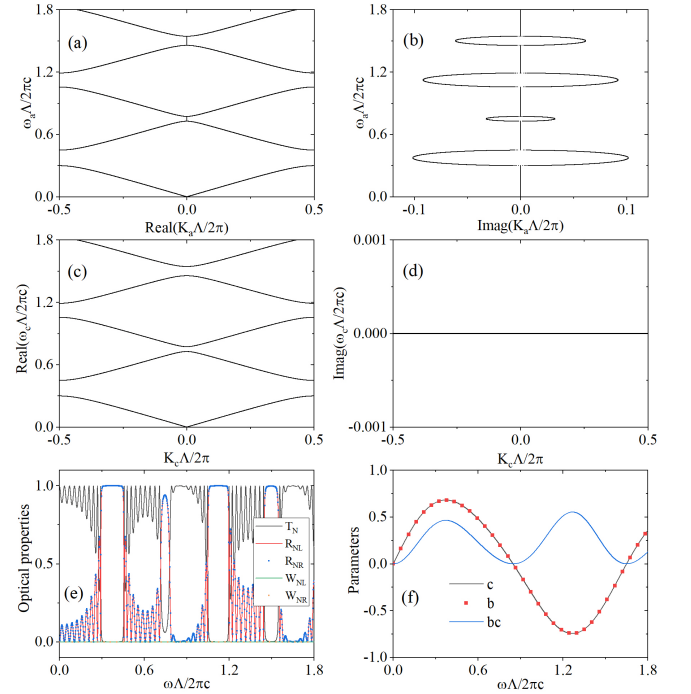


Figure 3. (Color online) Real ((a), (b)) and complex ((c), (d)) band structures of the 1DPTSPC in the absence of gain and loss ($\epsilon'' = 0$). (e) Optical properties T_N , R_{NL} , R_{NR} , W_{NL} and W_{NR} as functions of the reduced frequency when $\epsilon'' = 0$. (f) Values of c , b and bc as functions of the reduced frequency when $\epsilon'' = 0$.

$$W_{NR} = \frac{bc - c^2}{bc + \sinh^2 K_{ai}\Lambda / \sinh^2 NK_{ai}\Lambda}. \quad (14e)$$

Compared with the case in Eq. (12), these quantities have the same expressions except that the sine function is replaced by the hyperbolic sine function. In a special case, at the band edge, where $K_a\Lambda = m\pi$, we have

$$T_N = \frac{1}{bcN^2 + 1}, \quad (15a)$$

$$R_{NL} = \frac{b^2}{bc + 1/N^2}, R_{NR} = \frac{c^2}{bc + 1/N^2}, \quad (15b)$$

$$W_{NL} = \frac{bc - b^2}{bc + 1/N^2}, W_{NR} = \frac{bc - c^2}{bc + 1/N^2}. \quad (15c)$$

So far, we have derived the analytic solutions for the physical quantities T_N , R_{NL} , R_{NR} , W_{NL} , and W_{NR} to determine the scattering, absorbing and radiating properties of 1DPTSPC.

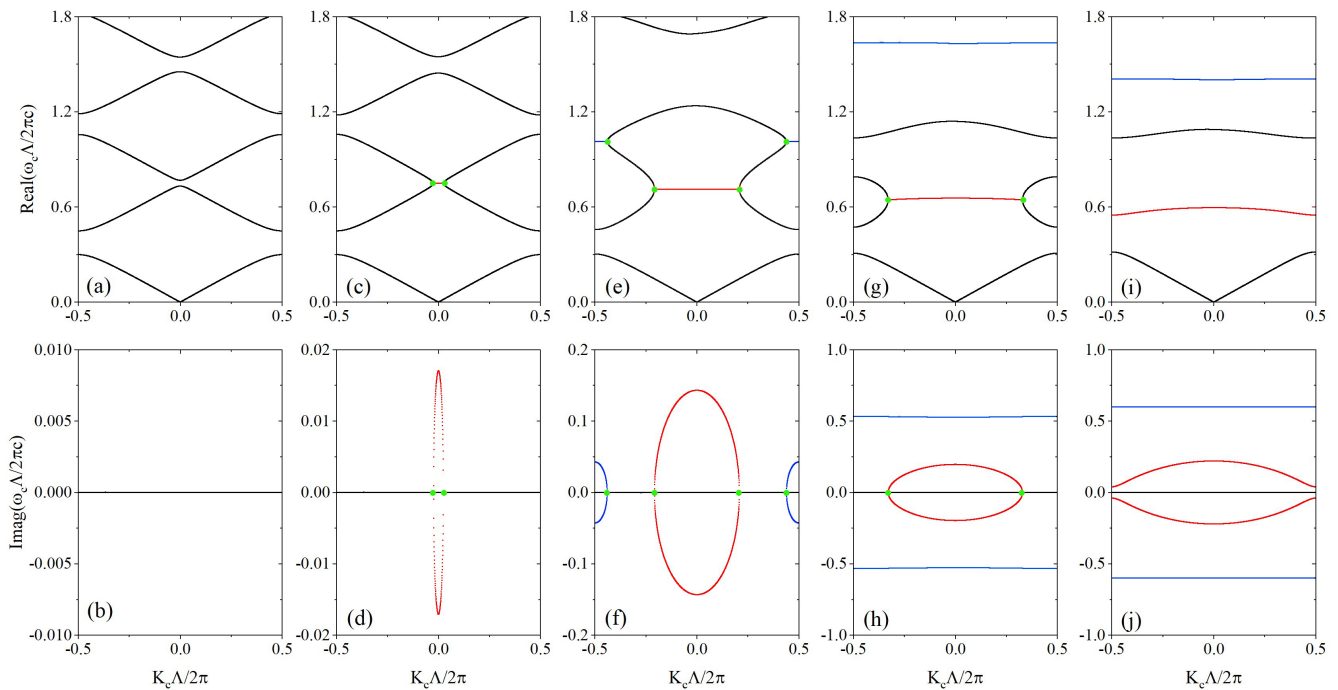


Figure 4. (Color online) Complex band structures of the 1DPTSPC for different values of ε'' . Top graphs: real parts of the complex eigenfrequencies. Bottom graphs: imaginary parts. (a)-(b): $\varepsilon'' = 0.1$. (c)-(d): $\varepsilon'' = 0.2$. (e)-(f): $\varepsilon'' = 1.0$. (g)-(h): $\varepsilon'' = 1.5$. (i)-(j): $\varepsilon'' = 2.0$. The black lines denote the eigenfrequencies are real, the other colored lines label complex eigenfrequencies. The green dots represent the exceptional points.

III. RESULT AND DISCUSSION

In this section, we discuss in detail the optical properties of 1DPTSPCs based on an analysis of its band structure. Figure 3 illustrates the real and complex band structures and the corresponding optical properties in the absence of gain and loss. In the conduction band regions, these two band structures coincide very well. However, in the band gap regions, the wave vector K_a for the real band structure becomes complex and the eigenfrequency ω_c for the complex band structure has no value. We emphasize that the 1DPTSPC here is also \mathcal{T} -symmetric, so $b = c$, $R_{NL} = R_{NR} \geq 0$ and $W_{NL} = W_{NR} = 0$, as derived from Eqs. (12) and (14). For every conduction band, $K\Lambda$ varies from 0 to π . There are $N - 1 = 9$ points where transmission resonances occur, because when $K\Lambda = n\pi/N$ ($n = 1, 2, \dots, N - 1$), then $\sin N K \Lambda / \sin K \Lambda = 0$, so $T_N = 1$ is obtained from Eq. (12a). At the same frequencies, the reflectances from both sides are zero, i.e. $R_{NL} = R_{NR} = 0$, as obtained from Eqs. (12b) and (12c). In the band gap, $\sinh^2 N K_{ai} \Lambda / \sinh^2 K_{ai} \Lambda$ is much larger than 1, so $T_N = 0$ is obtained from Eq. (14a), while $R_{NL} = R_{NR} = 1$ is obtained from Eqs. (14b) and (14c).

In Fig. 4, we present the complex band structures for different values of the imaginary relative permittivity ε'' . In our calculation, the 16 lowest bands in the absence of gain and loss are used to expand the Bloch waves in the corresponding \mathcal{PT} -symmetric photonic crystal. For

small values of ε'' , e.g. $\varepsilon'' = 0.1$ in Figs. 4(a) and 4(b), the eigenfrequencies for all the bands remains real. When ε'' is increased to a critical value, the first band gap starts to vanish and the 1st and 2nd bands begin to coalesce, in which case an exceptional point emerges at the center of the Brillouin zone. As ε'' is further increased, the previous exceptional point at the center is split in two, e.g. $\varepsilon'' = 0.2$ in Figs. 4(c) and 4(d). There points are located at either sides of the Brillouin center; between these two exceptional points the complex eigenfrequencies emerge, which are conjugate to each other. The band region with complex eigenfrequencies forms the \mathcal{PT} -broken phase, while the band region with real eigenfrequencies corresponds to the \mathcal{PT} -exact phase. These properties agree with non-Hermitian quantum mechanics.

If ε'' is further increased, the exceptional points which originate from the coalescence of the 3rd and 4th bands emerge at the Brillouin edge; at this time, the corresponding \mathcal{PT} -broken phase expands, as evident from Figs. 4(e) and 4(f). If we further increase ε'' beyond 1.0, the 2nd band gap reopens and the \mathcal{PT} -broken phase, which originates from the coalescence of the 2nd and 3rd band expansions, emerges at the Brillouin center and evolves into a band where the eigenvalues are all complex conjugates for all Bloch wave vectors. The \mathcal{PT} -broken phase, which originates from the coalescence of the 3rd and 4th bands, emerges at the Brillouin edge and then expands; this expansion then stops at some critical value of ε'' , after which this \mathcal{PT} -broken phase is decreased and

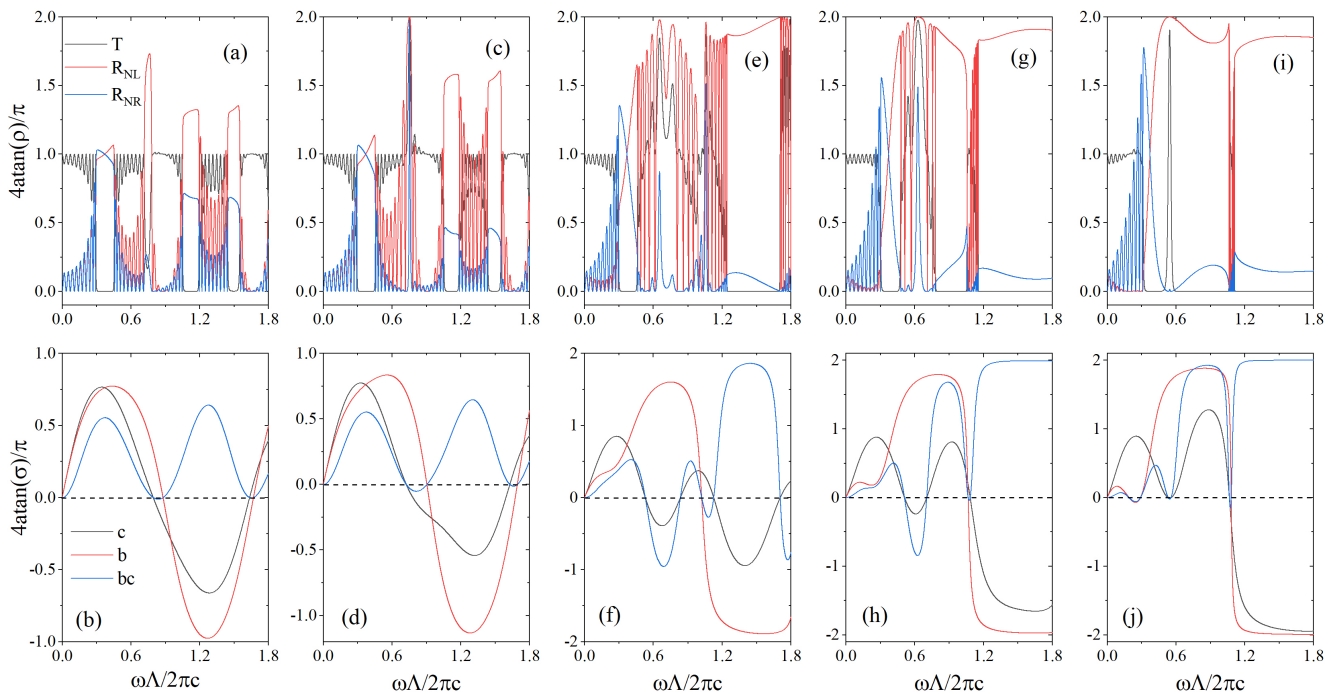


Figure 5. (Color online) Transmittance (T_N) and reflectances (R_{NL} and R_{NR}) of the 1DPTSPC with $N = 10$ periods. T_N , R_{NL} and R_{NR} are denoted by the black, red and blue lines in the top five panels, c , b and bc are marked by the black, red and blue lines in the bottom five panels. (a)-(b): $\varepsilon'' = 0.1$. (c)-(d): $\varepsilon'' = 0.2$. (e)-(f): $\varepsilon'' = 1.0$. (g)-(h): $\varepsilon'' = 1.5$. (i)-(j): $\varepsilon'' = 2.0$.

finally evolves into a completely real band. These phenomena can be seen in Figs. 4(g), (h), (i) and (j). Some of these preceding discussions are disclosed in [33]; here we investigate further the behaviour of the complex bands after ε'' is increased beyond 1.0.

Through the complex band structure, we can distinguish the \mathcal{PT} -exact and \mathcal{PT} -broken phases easily. However, in order to explain the optical properties thoroughly, we also depict the corresponding real band structures, which are shown in Appendix A. In fact, the part of the complex band structure with real eigenfrequency coincides with the part of the real band structure with a real Bloch wave vector. We can identify the band gap of the complex band structure, which is located at the gap between the real parts of two adjacent bands.

Figure 5 shows the transmittance, reflectances from both sides and parameters b , c and bc for different values of ε'' . Here, the number of unit cells is chosen to be $N = 10$. Because the values of the optical properties (T_N , R_{NL} , R_{NR} , W_{NL} and W_{NR}) are very large at some frequencies, in order to observe their variation we take the ordinate as $y = \frac{4}{\pi} \tan^{-1} \rho$, where ρ denotes the values of these optical properties. In this scale, if ρ is positive (negative), then y is also positive (negative). More than that, if $\rho = 1$, then $y = 1$, while if ρ tends to $\pm\infty$, y tends to ± 2 . For the same reason, we also take the ordinate as $\frac{4}{\pi} \tan^{-1} \sigma$ for the parameters we study, where σ denotes the values of the parameters. Combined with Figs. 4 and 5, it can be easily seen that these properties are closely related to the band structure. For some conduction bands

whose all eigenstates in the band structure are in the \mathcal{PT} -exact phase, $K\Lambda$ varies from 0 to π . In addition to the premise that b and c are finite, there are $N - 1 = 9$ points where transmission resonances occurs. This phenomenon also appears when $\varepsilon'' = 0$ in Fig. 3. For $\varepsilon'' \neq 0$, a part of a complex conduction band with real frequencies may be not complete, that is to say, the corresponding $K\Lambda$ only varies in a part of $[0, \pi]$. Consequently, in this band region there are fewer than $N - 1 = 9$ points corresponding to the transmission resonances. In the band gap, the transmittance is zero, i.e. $T_N = 0$, so $\sqrt{R_L R_R} = 1$ can be derived from the generalized conservation law, that means, either of R_{NL} and R_{NR} is greater than 1 and the other is less than 1, or both are equal to 1.

As can be seen from Figs. 4 and 5, near the position where the exceptional point occurs, bc becomes negative, so from Eq. (12a) the transmittance T_N is larger than 1. Moreover, if $\sin^2 NK\Lambda / \sin^2 K\Lambda$ approach $|1/bc|$, in some cases, the transmittance T_N can reach a very large value, and due to the generalized conservation law, one or both of R_{NL} and R_{NR} will also take large values. For example, when $\varepsilon'' = 0.2$, T_N reaches 689.35, R_{NL} and R_{NR} reach 8804.24 and 53.82, respectively, as shown in Fig. 5(c). However, in other conduction band regions and all the band gaps, T_N , R_{NL} and R_{NR} do not all reach large values simultaneously, because in these regions bc is greater than zero, so, as a result of Eq.(12a), T_N cannot be great than 1. At a frequency of 0.545 in Fig. 5(i), $T_N = 13.79 > 1$; however, bc here is positive. This seems to violate Eq. (12a); it actually does not, because there is an

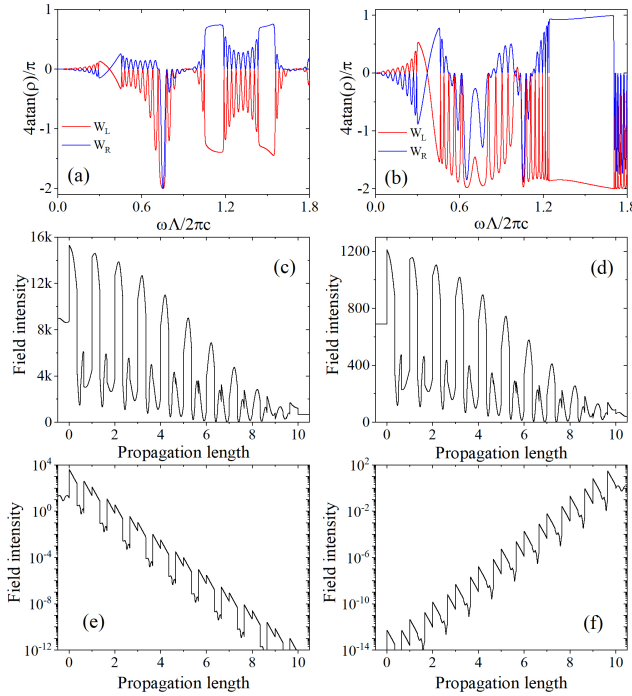


Figure 6. (Color online) Absorptance spectra (W_{NL} and W_{NR}) of the 1DPTSPC with $N = 10$ periods at (a) $\varepsilon'' = 0.2$ and (b) $\varepsilon'' = 1.0$. Field intensity distribution inside the \mathcal{PT} -symmetric photonic crystal is shown for incidence from the left side ((c) and (e)) and right side ((d) and (f)). The reduced frequency $\omega\Lambda/2\pi c = 0.75352$ and $\varepsilon'' = 0.2$ are chosen for (c) and (d), $\omega\Lambda/2\pi c = 1.5$ and $\varepsilon'' = 1.0$ for (e) and (f), respectively.

exceptional point near this frequency, which is not shown in the complex band structure because the computational method we use here is approximate, while it is apparent in the real band structure in Appendix A, which was obtained using a more accurate method.

In the band gap, as ε'' is increased from 0 to 2.0, the gap between R_{NL} and R_{NR} becomes very large. When ε'' is greater than 0.5, we see that R_{NL} is very large and R_{NR} is very small. We refer to the phenomenon where the reflectance from one side is small and that from the other side is large as unidirectional weak visibility. There are some similarities and differences between this phenomenon and unidirectional invisibility. In unidirectional invisibility [15–19], the reflectance from one side is zero and reflectance from the other side is one. However, in our phenomenon, the reflectance from one side is also very small but not zero, while the reflectance from the other side is also very large. More than that, in unidirectional invisibility the transmittance is one, while in our phenomenon it is zero and occurs in the band gap. This is a significant difference from unidirectional invisibility. For example, R_{NL} is greater than 9.28 and R_{NR} is less than 0.108 in the second band gap ($1.245 < \text{reduced frequency} < 1.7$) for $\varepsilon'' = 1.0$, while R_{NL} is greater than 7.5 and R_{NR} is less than 0.133 in the second band gap

($1.16 < \text{reduced frequency} < 1.89$) for $\varepsilon'' = 1.5$. The unidirectional weak visibility in the band gap is present for a wide frequency range.

It can be also seen from Fig. 4 that as ε'' is increased, flat bands with a narrow frequency range emerge. Some are real bands, for example as ε'' increases from 1.5, the second completely real band becomes flat and narrower and narrower. In Fig. 5, we see obvious resonances in this region. At both sides of this band, there are two large band gaps. By taking advantage of this property, the \mathcal{PT} -symmetric photonic crystal can be used as a filter, as only waves with frequencies in this narrow range can pass through it. The flat band in non-Hermitian system is also disclosed in other references [40, 41].

In addition to the study on the scattering properties, we also plot the absorptances with incidence from the left and right sides in Figs. 6(a) and (b) when $\varepsilon'' = 0.2$ and $\varepsilon'' = 1.0$, respectively. It can be seen from Fig. 6(a) that near the exceptional point bc is negative, W_L reaches -9492.6 and W_R reaches -742.2 at the same time, which means the optical effect of the 1DPTSPC from both sides is amplification. For the first band gap, the lines of W_{NL} and W_{NR} cross each other, as shown in Figs. 6(a) and (b). Actually, this phenomenon also happens for all ε'' we consider. This is also illustrated through Eqs. (14d) and (14e). bc is greater than zero at this region, and b is not equal to c in general; the denominators of W_{NL} and W_{NR} are equal, so if one of their enumerators is more than zero, then the other must be less than zero, so W_{NL} and W_{NR} have different signs. At the cross point $b = c$, so it can be easily seen from Eqs. (14d) and (14e) that $W_{NL} = W_{NR} = 0$. In general, when bc is larger than zero, these two absorptances have opposite signs, while when bc is less than zero, these two absorptances are both negative.

We also investigate the field intensity distribution in the 1DPTSPC when the light is incident from the left and right sides. In Figs. 6(c) and (d), we plot the field intensity distribution when the reduced frequency is chosen near the exceptional point for $\varepsilon'' = 0.2$. It can be easily seen that when the light is incident from the left side, the field intensity decays along the propagation direction; from the right side, the field intensity grows along the propagation direction. The field intensity distribution when the reduced frequency is fixed at the band gap is also considered in Figs. 6(e) and (f). We find that the field intensity decays sharply along the propagation direction when light in the band gap is incident from both sides, so the logarithmic coordinate is used to denote the variation. These phenomena agree with our preceding discussions.

IV. CONCLUSION

We have defined the generalized absorptance to include the amplification effect of the active dielectric, derived the mathematical expressions of the optical properties of

the 1DPTSPC, and expounded and analyzed these optical properties. Combined with the band structure, we find that some singular behaviors appear near the exceptional points, namely that the transmittance and reflectances from both sides are greater than one and all reach large values simultaneously, while the corresponding absorptances from both sides become negative. In the band gap, we observe unidirectional weak visibility, as the transmittance is zero and the reflectance is very large from one side, while the reflectance from the other side is very small. Based on this study, we envision various applications in the designs of functional optical devices, such as filters, switches, lasers and sensors.

ACKNOWLEDGMENTS

This work is supported by the National Natural Science Foundation of China (Grant No. 12004231), the Science and Technology Innovation Planning Project in Universities and Colleges of Shanxi Province of China (Grant No. 2019L0019), and the Applied Basic Research Program of Shanxi Province of China (Grant No. 201901D211165).

Appendix A: Optical properties of 1DPTSPC at higher frequencies

In Fig. 7, we present the real band structure corresponding to the complex band structure in Fig. 4 in the main text. After comparing these figures, we find that the part of the complex band structure with real eigenfrequencies coincides with the part of the real band structure with real Bloch wave vectors, while the parts with a complex Bloch wave vector correspond to the band gaps. When $\varepsilon'' = 2.0$, it can be seen from Figs. 7(i) and (j) that there are some parts of the conduction band structure with a real Bloch wave vector near the reduced frequency 0.56, but this is not evident in Figs. 4(i) and (j), which explains the sharp transmittance in Fig. 5(i) near the reduced frequency 0.56.

We also consider the cases when ε'' continues to be increased above 2.0. Figure 8 shows the evolution of the complex band structures when ε'' is 4.0, 6.5, 7.0, 8.0 and

12.0. In Fig. 8(a), the real part of the first complex band starts to move down and intersects with the first real band. As ε'' is increased to a critical value, the eigenfrequencies at two cross points become real, as shown in Figs. 8(c) and (d); that is to say, these two bands start to coalesce at these two cross points, which correspond to exceptional points. When ε'' is increased further, as shown in Figs. 8(e)-(h), each exceptional point splits into two; the middle part belongs to the real band, the first real band starts to coalesce with the second one, exceptional points are generated at the Brillouin edge and then move to its center. In this progression, the second real band disappears and a complex band is generated. As can be seen from Figs. 8(g)-(j), as ε'' is increased, all the high bands are in the \mathcal{PT} -broken phase, except the circle part of the band with low eigenfrequencies, which is in the \mathcal{PT} -exact phase. Moreover, this region decreases gradually with the further increase of ε'' and disappears altogether when ε'' is increased continuously beyond another critical value. Meanwhile, the only two exceptional points move to the center of Brillouin zone and then merge at this position, so all the bands belong to the \mathcal{PT} -broken phase. The corresponding real band structure is presented in Fig. 9, whose consistency can be also easily seen for these two band structures.

The corresponding transmittance, reflectances and parameters b , c and bc are presented in Fig. 10 for different values of ε'' . Here the number of unit cells is also fixed at $N = 10$. These values may also be very large, so we also take the ordinate as $\frac{4}{\pi} \tan^{-1} \rho(\sigma)$. We also observe similar phenomena to those described in Fig. 5 of the main text. If the incident light is located near the exceptional point, where “near” in this case means that the frequency or ε'' is taken near the corresponding values of the exceptional point, the transmittance, and reflectances may be much larger than one simultaneously. If the frequency or ε'' is not located near the exceptional point, then T_N , R_{NL} and R_{NR} cannot reach large values simultaneously. Moreover, we also observe perfect resonances at almost perfect flat bands. For example, it can be seen from Fig. 10(a) and (c) that the resonances occur when the reduced frequencies are 0.95 and 0.66, respectively. The absolute values of b and c at the band gap become larger and larger as ε'' is increased.

-
- [1] R. El-Ganainy, K. G. Makris, M. Khajavikhan, Z. H. Musslimani, S. Rotter, and D. N. Christodoulides, *Nat. Phys.* **14**, 11 (2018).
 - [2] L. Feng, R. El-Ganainy, and L. Ge, *Nat. Photonics* **11**, 752 (2017).
 - [3] N. Moiseyev, *Non-Hermitian Quantum Mechanics* (Cambridge University Press, 2011).
 - [4] C. M. Bender and S. Boettcher, *Phys. Rev. Lett.* **80**, 5243 (1998).
 - [5] C. M. Bender, D. C. Brody, and H. F. Jones, *Phys. Rev. Lett.* **89**, 270401 (2002).
 - [6] C. M. Bender, S. Boettcher, and P. N. Meisinger, *J. Math. Phys.* **40**, 2201 (1998).
 - [7] C. Hahn, E. K. Keshmarzi, S. H. Song, C. H. Oh, R. N. Tait, and P. Berini, *IEEE J. Sel. Top. Quant.* **22**, 48 (2016).
 - [8] J. Gu, X. Xi, J. Ma, Z. Yu, and X. Sun, *Sci. Rep.* **6**, 37688 (2016).
 - [9] L. Jin and Z. Song, *Phys. Rev. Lett.* **121**, 073901 (2018).
 - [10] M. A. Miri and A. Alù, *Science* **363**, eaar7709 (2019).

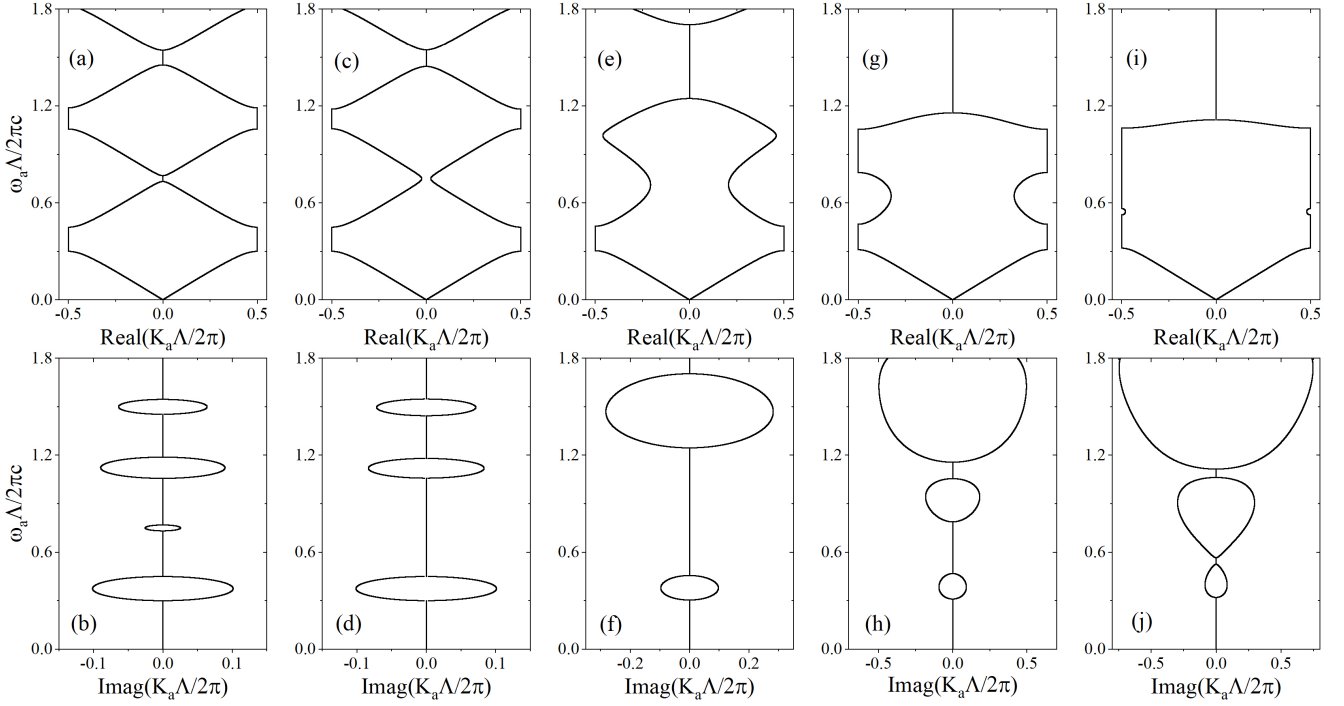


Figure 7. Real band structures of the 1DPTSPC. The top five graphs show the real parts of the Bloch wave vectors, and the bottom five graphs denote the corresponding imaginary parts. (a)-(b): $\epsilon'' = 0.1$. (c)-(d): $\epsilon'' = 0.2$. (e)-(f): $\epsilon'' = 1.0$. (g)-(h): $\epsilon'' = 1.5$. (i)-(j): $\epsilon'' = 2.0$.

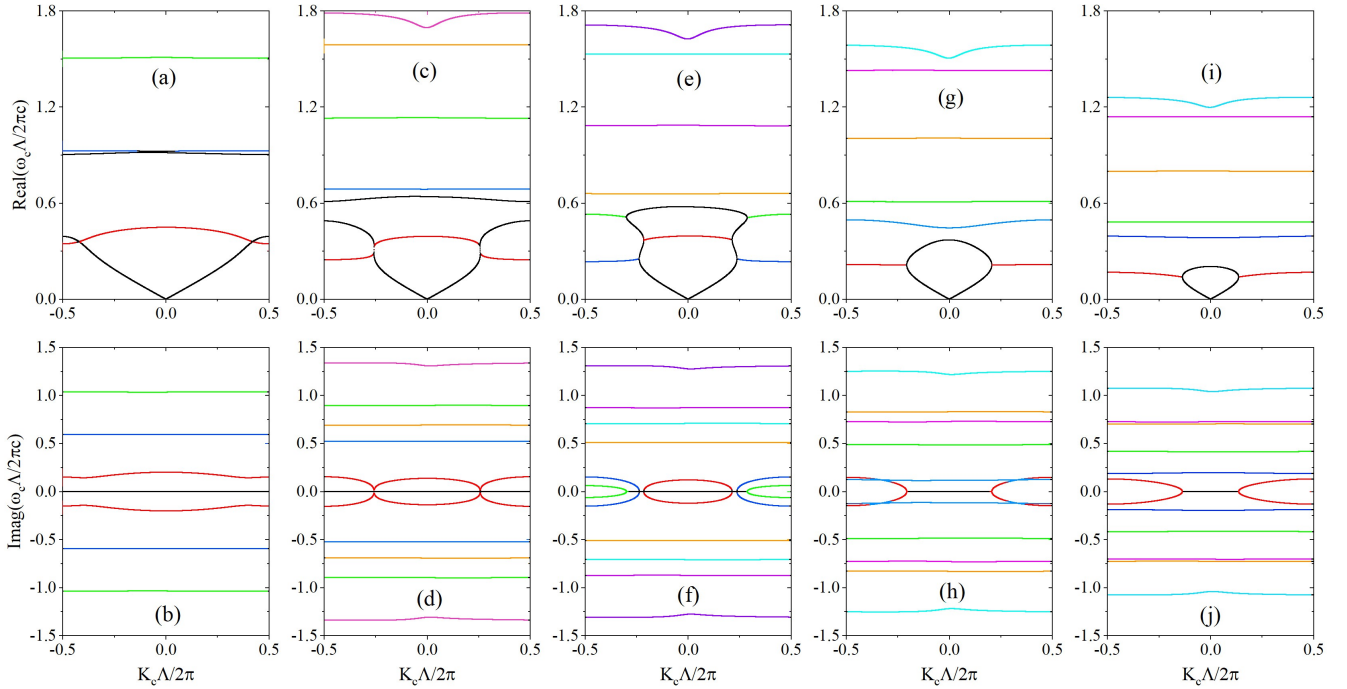


Figure 8. (Color online) Complex band structures of the 1DPTSPC for various values of ϵ'' . Top graphs: real parts of the complex eigenfrequencies. Bottom graphs: imaginary parts. (a)-(b) $\epsilon'' = 4.0$. (c)-(d) $\epsilon'' = 6.5$. (e)-(f): $\epsilon'' = 7.0$. (g)-(h): $\epsilon'' = 8.0$. (i)-(j): $\epsilon'' = 12.0$. All other parameters are identical to those in Fig. 3 of the main text.

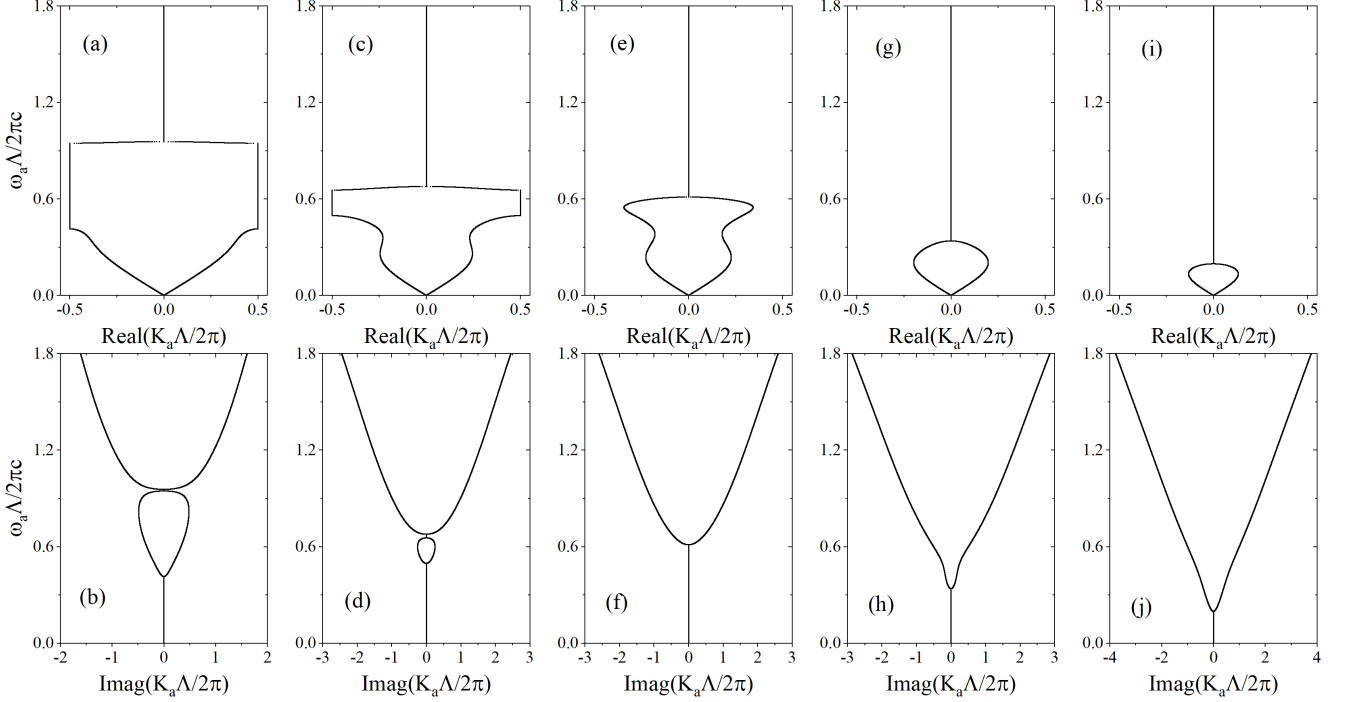


Figure 9. Real band structures of the 1DPTSPC for various values of ε'' . The top five graphs show the real parts of the Bloch wave vectors, while the bottom five graphs show the corresponding imaginary parts. (a)-(b) $\varepsilon'' = 4.0$. (c)-(d): $\varepsilon'' = 6.5$. (e)-(f): $\varepsilon'' = 7.0$. (g)-(h): $\varepsilon'' = 8.0$. (i)-(j): $\varepsilon'' = 12.0$.

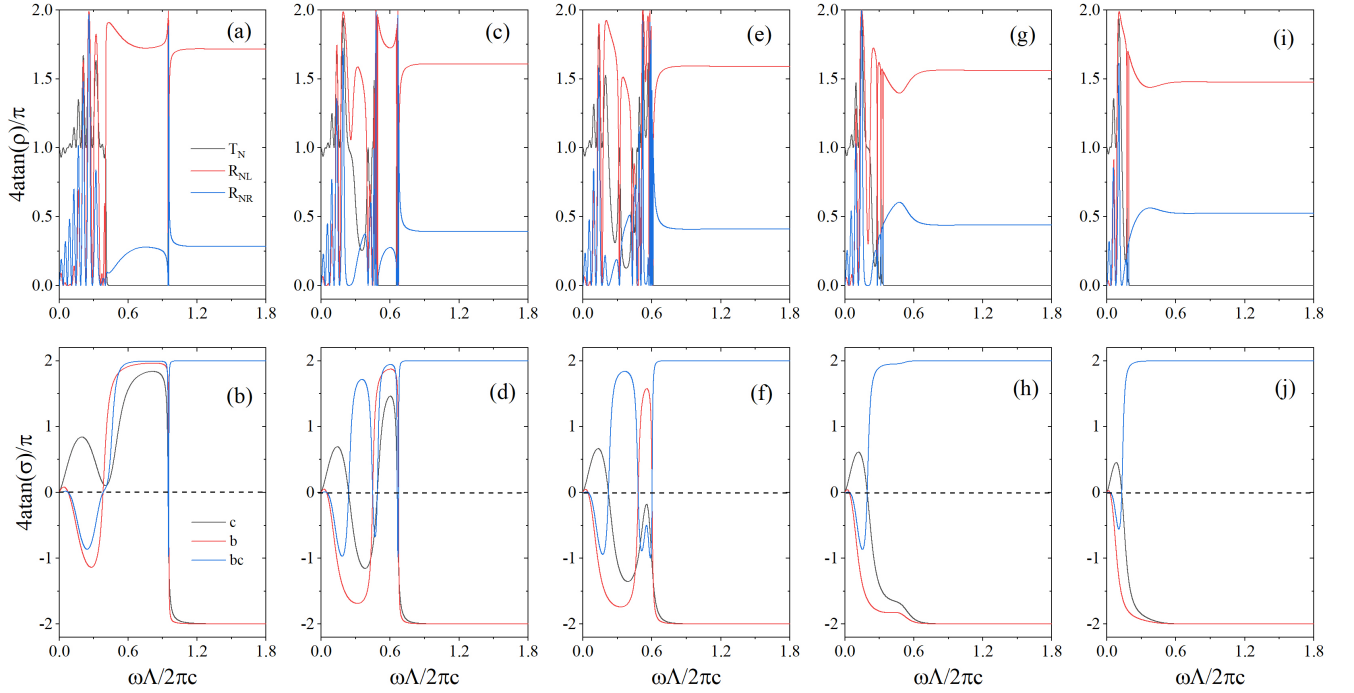


Figure 10. (Color online) Transmittance (T_N) and reflectances (R_{NL} and R_{NR}) of the 1D \mathcal{PT} -symmetric photonic crystal with $N = 10$ periods for various values of ε'' . T_N , R_{NL} and R_{NR} are denoted by the black, red and blue lines in the top five panels, while c , b and bc are marked by the black, red and blue lines in the bottom five panels. (a)-(b) $\varepsilon'' = 4.0$. (c)-(d): $\varepsilon'' = 6.5$. (e)-(f): $\varepsilon'' = 7.0$. (g)-(h): $\varepsilon'' = 8.0$. (i)-(j): $\varepsilon'' = 12.0$.

- [11] H. Ramezani, T. Kottos, V. Kovanis, and D. N. Christodoulides, *Phys. Rev. A* **85**, 153 (2012).
- [12] Z. Xu-Lin and C. T. Chan, *Phys. Rev. A* **98**, 033810 (2018).
- [13] Y. X. Xiao, Z. Q. Zhang, Z. H. Hang, and C. T. Chan, *Phys. Rev. B* **99**, 241403 (2019).
- [14] W. D. Heiss, *J. Phys. A* **37**, 2455 (2003).
- [15] Z. Lin, H. Ramezani, T. Eichelkraut, T. Kottos, H. Cao, and D. N. Christodoulides, *Phys. Rev. Lett.* **106**, 213901 (2011).
- [16] V. A. Bushuev, D. M. Tsvetkov, V. V. Konotop, and B. I. Mantsyzov, *Opt. Lett.* **44**, 5667 (2019).
- [17] C. E. Rüter, K. G. Makris, R. El-Ganainy, D. N. Christodoulides, M. Segev, and D. Kip, *Nat. Phys.* **6**, 47 (2010).
- [18] L. Feng, Y. L. Xu, W. S. Fegadolli, M. H. Lu, J. E. B. Oliveira, V. R. Almeida, Y. F. Chen, and A. Scherer, *Nat. Mater.* **12**, 108 (2013).
- [19] X. F. Zhu, Y. G. Peng, and D. G. Zhao, *Opt. Express* **22**, 18401 (2014).
- [20] H. Ramezani, T. Kottos, R. El-Ganainy, and D. N. Christodoulides, *Phys. Rev. A* **82**, 043803 (2010).
- [21] S. Longhi, *Phys. Rev. A* **82**, 9583 (2010).
- [22] L. Feng, Z. J. Wong, R. Ma, Y. Wang, and X. Zhang, *Science* **346**, 972 (2014).
- [23] Z. J. Wong, Y. L. Xu, J. Kim, K. O'Brien, Y. Wang, L. Feng, and X. Zhang, *Nat. Photonics* **10**, 796 (2016).
- [24] H. Hodaei, M. A. Miri, M. Heinrich, D. N. Christodoulides, and M. Khajavikhan, *Science* **346**, 975 (2014).
- [25] M. Farhat, M. Yang, Z. Ye, and P.-Y. Chen, *ACS Photonics* **7**, 2080 (2020).
- [26] Y. D. Chong, L. Ge, and A. D. Stone, *Phys. Rev. Lett.* **106**, 093902 (2011).
- [27] L. Ge and L. Feng, *Phys. Rev. A* **94**, 043836 (2016).
- [28] L. Ge, Y. D. Chong, and A. D. Stone, *Phys. Rev. A* **85**, 445 (2012).
- [29] A. Y. Song, Y. Shi, Q. Lin, and S. Fan, *Phys. Rev. A* **99**, 013824 (2019).
- [30] H. Alaeian and J. A. Dionne, *Phys. Rev. B* **89**, 188 (2014).
- [31] J. Schnabel, H. Cartarius, J. Main, G. Wunner, and W. D. Heiss, *Phys. Rev. A* **95**, 053868 (2017).
- [32] R. El-Ganainy, K. G. Makris, D. N. Christodoulides, and Z. H. Musslimani, *Opt. Lett.* **32**, 2632 (2007).
- [33] K. Ding, Z. Q. Zhang, and C. T. Chan, *Phys. Rev. B* **92**, 235310 (2015).
- [34] Z. L. Zhen, F. Qin, Z. Qiang, and J. J. Xiao, *Opt. Express* **25**, 26689 (2017).
- [35] A. Cerjan, A. Raman, and S. Fan, *Phys. Rev. Lett.* **116**, 203902 (2016).
- [36] Y. Amnon and P. Yeh, *Optical waves in crystals: propagation and control of laser radiation* (New York City, NY: Wiley, 1984).
- [37] K. Sakoda, *Optical properties of photonic crystals* (Springer Science & Business Media, 2004).
- [38] P. Yeh, A. Yariv, and C.-S. Hong, *J. Op. Soc. Am.* **67**, 423 (1977).
- [39] A. Yariv and P. Yeh, *J. Op. Soc. Am.* **67**, 438 (1977).
- [40] H. Ramezani, *Phys. Rev. A* **96**, 011802 (2017).
- [41] Z. Liu, Q. Zhang, F. Qin, Y. Chen, and J. J. Xiao, *Phys. Rev. A* **98**, 043844 (2018).